GFZ
Helmholtz-Zentrum
POTSDAM

HELMHOLTZ-ZENTRUM POTSDAM
DEUTSCHES
GEOFORSCHUNGSZENTRUM

Peng, C., Li, S., Wu, W., An, H., Chen, X., Ouyang, C., Tang, H. (2022): On three-dimensional SPH modelling of large-scale landslides. - Canadian Geotechnical Journal, 59, 1, 24-39.

https://doi.org/10.1139/cgj-2020-0774

Copyright © 2022 Canadian Science Publishing
© 2021 The Author(s). Permission for reuse (free in most cases) can be obtained from copyright.com.

Institional Repository GFZpublic: https://gfzpublic.gfz-potsdam.de/

Canadian Science Publishing | Canadian Geotechnical Journal

On three-dimensional SPH modelling of large-scale landslides

Journal:	*Canadian Geotechnical Journal*
Manuscript ID	cgj-2020-0774
Manuscript Type:	Article
Date Submitted by the Author:	20-Dec-2020
Complete List of Authors:	Peng, Chong; Universität für Bodenkultur Wien, Institute of Geotechnical Engineering Li, Shuai; Chinese Academy of Sciences; Deutsches Geoforschungszentrum Potsdam Wu, Wei; Universität für Bodenkultur Wien An, Huicong; Chinese Academy of Sciences Chen, Xiaoqing; Chinese Academy of Sciences Ouyang, Chaojun; Chinese Academy of Sciences Tang, Hui; Deutsches Geoforschungszentrum Potsdam
Keyword:	Large-scale landslides, smoothed particle hydrodynamics, constitutive model, GPU acceleration, convergence
Is the invited manuscript for consideration in a Special Issue? :	Not applicable (regular submission)

SCHOLARONE™
Manuscripts

© The Author(s) or their Institution(s)

On three-dimensional SPH modelling of large-scale landslides

Chong Peng[a], Shuai Li[b,c], Wei Wu[a,*], Huicong An[b], Xiaoqing Chen[b], Chaojun Ouyang[b], Hui Tang[c]

[a]*Institut für Geotechnik, Universität für Bodenkultur, 1180 Vienna, Austria*
[b]*Key Laboratory of Mountain Hazards and Earth Surface Process, Institute of Mountain Hazards and Environment, Chinese Academy of Sciences, 610041 Chengdu, China*
[c]*Section 4.7: Earth Surface Process Modelling, German Research Centre for Geosciences (GFZ), 14473 Potsdam, Germany*

Abstract

Lagrangian particle-based smoothed particle hydrodynamics (SPH) is more and more widely used in landslide modelling. This paper investigates four important issues not addressed by previous studies on SPH modelling of large-scale landslides, i.e. convergence property, influence of constitutive parameters, scale effect and friction reduction, and the influence of different treatments of the viscous effect. GPU-acceleration technique is employed to achieve high-resolution 3D modelling. The Baige landslide is investigated by comparing numerical results with field data, and detailed analyses on the four issues are provided. Suggestions on particle resolution, constitutive parameter, and formulations of viscous discretization are also presented for future SPH modelling of large-scale landslides.

Keywords: Large-scale landslides, smoothed particle hydrodynamics, constitutive model, GPU acceleration, convergence

Draft

1. INTRODUCTION

Large-scale landslides are a major socio-economic threat in mountainous regions, as they usually lead to continuous damage of infrastructures and, in many cases, causalities. Various numerical methods were applied to landslide modelling by researchers with the aim of, among others, investigating the mechanism of landslide evolution, predicting affected area and impact [1–3], and assisting the design of mitigation measurements [4, 5]. As landslides involve large deformation of geomaterials, conventional mesh-based methods have numerical difficulties caused by distorted or tangled mesh; thus, they are not suitable to simulate landslides unless additional treatments such as constant remeshing [6] or interface tracking [7] are employed.

Alternatively, smoothed particle hydrodynamics (SPH) is a meshless Lagrangian particle method, which can model large deformation, moving interface, and material separation and fragmentation naturally without any special treatments. Consequently, SPH was applied to a wide range of applications including dynamic fluid flows [8, 9], large deformation analysis of material with strength [10–13], cracking modelling [14, 15], and impact and explosion [16–19], among others.

Owing to the advantages described above, SPH is suitable for modelling landslides and has been gaining popularity recently. Based on the depth-integration approach, Pastor and co-authors [2, 20–22] developed efficient depth-integrated SPH models for run-out analysis of large-scale landslides, in which various basal friction models and soil-water coupling conditions can be considered. On the other hand, more general full dimensional simulations employing complete conservative equations also attracted many attentions. For instance, SPH was widely used to simulate small-scale mass movements including granular flow [23–25], sand collapse [26, 27], and small-scale landslides [10, 11, 28]. In these studies, the flowing materials are modelled as single-phase with rheological or elastoplastic constitutive models. The considered problems are small-scale with size usually smaller than several meters. It is generally observed that in small-scale problems SPH can provide numerical results well corroborated by experiments; thus, it proves to be a capable and reliable numerical tool.

*Corresponding author. E-mail: wei.wu@boku.ac.at

© The Author(s) or their Institution(s)

Many researchers also employed SPH to model large-scale landslides on real terranes. For instance, Huang et al. [29] and Hu et al. [30] performed 2D and 3D simulations of several large-scale landslides in the Wenchuan earthquake area, where realistic terranes were generated using Digital Elevation Models (DEMs). Dai and co-authors [31, 32] developed 3D SPH model for large-scale landslides and investigated run-out and interaction with structures. Zhu et al. [33] modelled the flow process of a landslide induced by landfill and studied the affected area. In these studies, the materials were modelled as non-Newtonian fluids with a Mohr-Coulomb type yield surface (Hereafter referred to as rheological MC model). The interactions between flowing masses and bed rocks were modelled using non-slip boundary condition. Wang et al. [34] employed the rheological Cross model [35] to model flow-like landslides, where the model parameters were derived by fitting the resulted viscosity from the Cross model and the rheological MC model. These studies show that SPH is able to capture the salient dynamic behaviours of large-scale landslides, and provides useful information for hazard analysis.

Nevertheless, it is observed that in SPH modelling of large-scale landslides there are several important issues not addressed by previous studies. First, high resolution 3D modelling and convergence analysis have yet not been reported. Some previous studies are based on 2D modelling; however, on complex real terranes it is uncertain whether 2D modelling can reflect real 3D flow dynamics. While some studies are based on 3D modelling, due to the high computational cost of SPH, the numerical resolutions are usually rather low and the total particle numbers are limited. More importantly, no convergence analysis was provided, indicating that the influence of numerical resolution is largely overlooked. Second, investigation on the influence of constitutive parameters is still missing. Third, if the material is modelled as non-Newtonian fluid, there exist two formulations to handle the viscous term, i.e. the full shear stress tensor formulation [29–31, 33] and the Morris-type viscosity formulation [36–38]. Assessment and comparison of these two formulations are not yet reported. Fourth, it is widely-acknowledged that for large-scale landslides the run-out distances are much longer than expected from the usual values of frictional coefficient obtained from laboratory tests [39–43]. That means, on the other hand, if the usual frictional coefficient obtained from laboratory (~0.5 - 0.7) are used in numerical simulations, the resulted run-out distances would be significantly underestimated [43, 44]. However, this scale effect has not been discussed in previous researches, probably with the only exception of Zhang et al. [45], where a velocity-based friction reduction law is employed to achieve reasonable run-out distance for a rockslide.

Owing to the recent advances on parallel computing of SPH, especially with GPU acceleration, large-scale SPH simulations with millions to dozens of millions of particles can be performed efficiently on desktop computers. Therefore, it is the right time to extensively investigate the aforementioned issues of SPH simulations of large-scale landslides. Such study is of significance because it can thoroughly check the capability of SPH, compare different formulations, study the influences of constitutive models and parameters, and investigate the scale effect unique to large-scale lanslides. By doing so, it can provide suggestions and references to future modelling. In this work, based on the open-source GPU-accelerated SPH solver LOQUAT [28], we will study the following aspects of SPH modelling of large-scale landslides: (1) the convergence behaviour of SPH in three-dimensional large-scale landslide modelling; (2) the influences of constitutive model parameters; (3) the influences of different treatments of the viscous effect; (4) the largely overlooked scale-effect and its impact on the simulation results.

2. GOVERNING EQUATIONS AND CONSTITUTIVE MODELS

2.1. Governing equations

The governing equations of mass movement consist of the classical mass and momentum conservation equations written in the following Lagrangian form

$$\frac{\mathrm{d}\rho}{\mathrm{d}t} = -\rho\nabla\cdot\mathbf{v} \tag{1}$$

$$\frac{\mathrm{d}\mathbf{v}}{\mathrm{d}t} = \frac{1}{\rho}\nabla\cdot\boldsymbol{\sigma} + \mathbf{g} \tag{2}$$

where ρ, $\mathbf{v}$, $\boldsymbol{\sigma}$, and $\mathbf{g}$ are the density, velocity, Cauchy stress tensor, and body force, respectively. $\mathrm{d}(\cdot)/\mathrm{d}t$ denotes the material derivative; ∇ is the gradient operator and $(\cdot)$ indicates the inner product.

© The Author(s) or their Institution(s)

If the moving mass is considered as fluid material, usually the Cauchy stress tensor is decomposed as

$$\boldsymbol{\sigma} = -p\mathbf{I} + \boldsymbol{\tau} \tag{3}$$

where p is the pressure and $\boldsymbol{\tau}$ is the shear stress tensor. For fluids, the shear stress is usually computed through

$$\boldsymbol{\tau} = 2\eta\dot{\boldsymbol{\varepsilon}} = \eta\left[\nabla\mathbf{v} + (\nabla\mathbf{v})^{\mathrm{T}}\right] \tag{4}$$

where $\dot{\boldsymbol{\varepsilon}} = 0.5\left[\nabla\mathbf{v} + (\nabla\mathbf{v})^{\mathrm{T}}\right]$ is the strain rate tensor with $\nabla\mathbf{v}$ being the velocity gradient, η is the dynamic viscosity.

Substituting Eqs. (3) and (4) into Eq. (2), we have

$$\frac{\mathrm{d}\mathbf{v}}{\mathrm{d}t} = -\frac{\nabla p}{\rho} + \frac{\eta\nabla^2\mathbf{v}}{\rho} + \frac{\eta\nabla\cdot(\nabla\mathbf{v})^{\mathrm{T}}}{\rho} + \mathbf{g} \tag{5}$$

It is found that the shear stress term can be rewritten into one term related to pure shear deformation and one accounting for the bulk viscosity. For incompressible fluids, the term for bulk viscosity is zero because $\nabla\cdot(\nabla\mathbf{v})^{\mathrm{T}} = \nabla(\nabla\cdot\mathbf{v}) = \mathbf{0}$. As a result, the momentum conservation equation for incompressible fluids can be written as

$$\frac{\mathrm{d}\mathbf{v}}{\mathrm{d}t} = -\frac{\nabla p}{\rho} + \frac{\eta\nabla^2\mathbf{v}}{\rho} + \mathbf{g} \tag{6}$$

Eq. (2) is valid for both fluid- and solid-based material models, whereas Eq. (6) is only for incompressible fluids. Utilizing Eqs. (2) and (6) results in different SPH formulations. which will be detailed in Section 3.

2.2. Constitutive model

Moving masses of landslides are complex multiphase material with soil, water, air, and large rocks; thus, accurate simulations would require the use of mixture or multiscale and multiphase models [46, 47]. As a first approximation, however, geomaterials in landslides are usually modelled as one single mixed material either with non-Newtonian rheological models or geomechanical constitutive models. In this work, we employ the rheological Mohr-Coulomb (MC) model, which is a non-Newtonian rheological model considering moving masses as fluids.

Usually, non-Newtonian rheological models only produces an apparent viscosity, which is then employed to compute the shear stress using Eq. (4). The remaining part of the Cauchy stress tensor, i.e. the pressure p, is usually obtained through an equation of state (EOS) based on the weakly-compressible assumption. The EOS employed in this work reads as follows

$$p = \frac{c_s^2\rho_0}{7}\left[\left(\frac{\rho}{\rho_0}\right)^7 - 1\right] \tag{7}$$

where c_s and ρ_0 are the speed of sound and reference density, respectively.

In landslides with considerable water contents and fine particles or under liquifacted state, the mass flow exhibits strong viscous behaviour and are sometimes modelled using the viscoplastic Bingham model [48–50]. In the Bingham model, there exists a yield stress τ_y which must be exceeded priori to motion. Once mobilized, the material flows with a plastic viscosity η_∞. However, for geometerials, the yielding condition is mainly controlled by friction; thus, the yield stress is pressure dependent. Using the Mohr-Coulomb yield condition, the yield stress can be written as

$$\tau_y = c + \mu p \tag{8}$$

where c is the cohesion, p is the pressure, and $\mu = \tan\phi$ denotes friction coefficient, where ϕ is the frictional angle.

In a flowing state, the total shear stress is

$$\tau = \tau_y + \eta_\infty\dot{\gamma} \tag{9}$$

where $\dot{\gamma}$ is the shear rate, which is defined as $\dot{\gamma} = \sqrt{2\dot{\boldsymbol{\varepsilon}} : \dot{\boldsymbol{\varepsilon}}}$ in three-dimensions. Based on Eq. (9), the apparent viscosity (the ratio between shear stress and shear rate) can be obtained as

© The Author(s) or their Institution(s)

$$\eta_{app} = \eta_\infty + \frac{c + \mu p}{\dot{\gamma}} \tag{10}$$

It is found that the above model is singular in the static state where $\dot{\gamma} = 0$. It also produces extremely high apparent viscosity in the quasi-static regime where $\dot{\gamma}$ is close to zero. To avoid numerical difficulties, the following regularization [51] is usually used in simulations

$$\eta_{app} = \eta_\infty + \frac{c + \mu p}{\dot{\gamma}} \left(1 - \mathrm{e}^{-m\dot{\gamma}}\right) \tag{11}$$

It is found in the regularized model the apparent viscosity becomes $\eta_\infty + m(c + \mu p)$ when $\dot{\gamma}$ approaches zero. m is a parameter with the unit of s^{-1}. The rheological MC model is probably the most widely-used constitutive model in SPH landslides and mass flows modelling [6, 7, 29–33, 38]. Compared with the apparent viscosity from the yield stress, the plastic viscosity η_∞ is very small. Therefore, in simulations of large-scale problems, the parameter η_∞ is usually neglected or taken as the viscosity of water [32, 38]. Therefore, the rheological MC model has three parameters: the friction coefficient μ, the cohesion c, and the regularization parameter m.

3. SPH FORMULATIONS

3.1. SPH approximation

In SPH simulation of landslides, the material are discretized as particles, which can be considered as material elements with fixed mass. The particles carry state variables, e.g. mass, velocity, density, and stress, and move with the material. The governing equations are solved based on the discrete Lagrangian particles. A field function $f(\mathbf{x})$ and its gradient $\nabla f(\mathbf{x})$ at particle $\mathbf{x}_i$ can be approximated through the discrete function values in the neighborhood of $\mathbf{x}_i$ with a SPH kernel function

$$f_i = \sum_{j=1}^{n} f_j W_{ij} \frac{m_j}{\rho_j} \tag{12}$$

$$\nabla f_i = \sum_{j=1}^{n} f_j \nabla_i W_{ij} \frac{m_j}{\rho_j} \tag{13}$$

where $f_i = f(\mathbf{x}_i)$ and $\nabla f_i = \nabla f(\mathbf{x}_i)$. n is the number of particles in the support domain of $\mathbf{x}_i$. f_j, m_j, and ρ_j are the function value, mass, and density of particle j. $W_{ij} = W(\mathbf{x}_i - \mathbf{x}_j, h)$ is the smoothing kernel, which depends on the distance between the two particles i and j, and the smoothing length h. In this work, the Wendland C2 kernel function [52] is employed. The radius of the support domain is $2h$, where h is taken as 1.35 times of the initial particle spacing Δr.

3.2. Discretization of the governing equations

With the SPH function approximation, the governing equations (1) and (2) can be written as the following common discretized form

$$\frac{\mathrm{d}\rho_i}{\mathrm{d}t} = \sum_{j=1}^{n} m_j (\mathbf{v}_i - \mathbf{v}_j) \cdot \nabla_i W_{ij} \tag{14}$$

$$\frac{\mathrm{d}\mathbf{v}_i}{\mathrm{d}t} = \sum_{j=1}^{n} m_j \left(\frac{\boldsymbol{\sigma}_i}{\rho_i^2} + \frac{\boldsymbol{\sigma}_j}{\rho_j^2} - \Pi_{ij}\mathbf{I} \right) \nabla_i W_{ij} + \mathbf{g}_i \tag{15}$$

where $\Pi_{ij} = \Pi_{ij}^v + \Pi_{ij}^p$ is the stabilization term consisting of the artificial viscosity Π_{ij}^v and artificial pressure Π_{ij}^p, which are employed to damp out unphysical numerical oscillations and mitigate the tensile instability, respectively. The detailed forms of the artificial viscosity and pressure can be found in the original papers of Monaghan [8, 53]; thus, they are omitted here.

© The Author(s) or their Institution(s)

The discreted governing equations (14) and (15) are widely used in SPH simulations of landslides and mass movements with elastoplastic models [10, 26, 54, 55]. They are also employed in simulations of large-scale landslides with rheological models [29–33], provided that the full stress tensors is constructed using pressures and shear stress tensors.

3.3. Discretization of the viscous Laplacian term

As shown in Section 2.1, if the geomaterial is considered as incompressible fluid using the rheological MC constitutive model, the momentum conservative equations can also be written as Eq. (6). In the modelling of granular flows and geophysical flows, direct discretization of the viscous Laplacian is also possible without computing the full stress tensor. With the incompressible assumption, the discrete momentum equation can be written as

$$\frac{\mathrm{d}\mathbf{v}_i}{\mathrm{d}t} = \sum_{j=1}^{n} m_j \left(\frac{p_i}{\rho_i^2} + \frac{p_j}{\rho_j^2} + \Pi_{ij}\mathbf{I} \right) \nabla_i W_{ij} + \mathbf{L}_i + \mathbf{g}_i \tag{16}$$

where $\mathbf{L}_i$ is the SPH discretized Laplacian, i.e. $\eta\nabla^2\mathbf{v}/\rho$. Based on the pioneer work of Brookshaw [56], Morris employed a SPH Laplacian discretization in laminar flow modelling by combining SPH and finite difference approximation [36]. Later, various Laplacian discretizations were proposed for laminar flows and non-Newtonian flows [57, 58]. Basa et al [58] reviewed common approaches of discretizing the Laplacian in SPH and found that the Morris-type formulation [36] gives best results in modelling low Reynolds number Newtonian flows. In literature, various Morris-type formulations are employed in simulation of geophysical flows. For instance, Hérault et al [37] employed a modified Morris-type discrete Laplacian in lava flow modelling. Szewc [38] used the original formulation from Morris to model granular flows. Shao et al [59] adopted a different version of Laplacian term in non-Newtonian flow modelling. Although various formulations of Laplacian discretization are employed, their influence on numerical results of geophysical flows has not been reported. In this work, the following three types of discrete Laplacian formulations are employed, and their performance are checked through numerical investigation.

$$\text{Original Morris type [36]: } \mathbf{L}_i = \sum_{j=1}^{n} \frac{m_j(\eta_i + \eta_j)\mathbf{r}_{ij} \cdot \nabla_i W_{ij}}{\rho_i \rho_j (r_{ij}^2 + 0.01h^2)} \mathbf{v}_{ij} \tag{17}$$

$$\text{Hérault et al [37]: } \mathbf{L}_i = \sum_{j=1}^{n} \frac{m_j}{\rho_i \rho_j} \frac{4\eta_i \eta_j}{\eta_i + \eta_j} \frac{\mathbf{r}_{ij} \cdot \nabla_i W_{ij}}{r_{ij}^2 + 0.01h^2} \mathbf{v}_{ij} \tag{18}$$

$$\text{Shao et al [59]: } \mathbf{L}_i = \sum_{j=1}^{n} \frac{4m_j(\eta_i + \eta_j)\mathbf{r}_{ij} \cdot \nabla_i W_{ij}}{(\rho_i + \rho_j)^2 (r_{ij}^2 + 0.01h^2)} \mathbf{v}_{ij} \tag{19}$$

where $\mathbf{r}_{ij} = \mathbf{x}_i - \mathbf{x}_j$ and $\mathbf{v}_{ij} = \mathbf{v}_i - \mathbf{v}_j$. Hereafter these forms are termed as 'LF (Laplacian formulation)-Morris', 'LF-Hérault', and 'LF-Shao', while Eq. (15) is referred to as 'stress-based formulation (SF)'. All the four forms were used in SPH modelling of large-scale landslides. It is easily found that generally the LFs use less memory and are more efficient than the SF, because the LFs do not need to store the full stress tensor or perform the calculations related to stress tensor. Detailed comparison between the these formulations are given in Section 8.

3.4. δ-SPH formulation

It is well-known that the classical SPH method suffers from the short-length-scale-noise, which results in fluctuations in pressure/stress fields [24, 60]. Although this noise has little influence on the kinematics, it may lead to inaccurate results of impacting forces on structures. In simulations with pressure-dependent constitutive model, e.g. the rheological MC model, this noise may also have greater impact due to inaccurate pressure results. To smooth out the pressure noise, in this paper the δ-SPH, a density diffusion term, is employed. With the δ-SPH term, the discretized continuity equation is written as

$$\frac{\mathrm{d}\rho_i}{\mathrm{d}t} = \sum_{j=1}^{n} m_j(\mathbf{v}_i - \mathbf{v}_j) \cdot \nabla_i W_{ij} + \delta h c_s \sum_{j=1}^{n} \frac{m_j}{\rho_j} \boldsymbol{\psi}_{ij} \cdot \nabla_i W_{ij} \tag{20}$$

© The Author(s) or their Institution(s)

where δ is a constant usually taken as 0.1 [61], $\boldsymbol{\psi}_{ij}$ has the following form

$$\boldsymbol{\psi}_{ij} = 2(\rho_i - \rho_j)\frac{\mathbf{r}_{ij}}{r_{ij}^2 + 0.01h^2} \tag{21}$$

4. IMPLEMENTATION AND GPU ACCELERATION

In this work, fixed non-slip boundaries are simulated using the boundary particle method [28, 62], in which boundaries are represented by certain layers (usually three) of boundary particles. These boundary particles are fixed in position and participate in the SPH computation like normal material particles, but their field variables such as velocity, density, viscosity, and stress/pressure are obtained by extrapolating from the neighboring material region.

The second-order predictor-corrector time integration scheme [8] is employed to solve the discretized governing equations. To ensure the stability of computations, the time step is computed based on the Courant-Friedrichs-Lewy (CFL)

$$\Delta t = \chi \min\left(\frac{h}{c_s}, \frac{h}{\max \|\mathbf{a}_i\|}\right) \tag{22}$$

where $\mathbf{a}_i = \mathrm{d}\mathbf{v}_i/\mathrm{d}t$ is the particle acceleration, χ is the CFL number with a custom range between 0.1 - 0.2 in SPH simulations. For simulations with non-Newtonian constitutive models, the time step has an additional restriction resulted from the viscous effect [63]

$$\Delta t = \chi \min\left(\frac{h}{c_s}, \frac{h}{\max \|\mathbf{a}_i\|}, h^2 \min \frac{\rho_i}{\eta_{app,i}}\right) \tag{23}$$

It can be observed that the restriction from the viscous effect may lead to extremely small time step in simulations with fine resolution and high viscosity. Fortunately, in simulations of large-scale landslides, typical numerical resolutions are greater than 1 m. Therefore, even the rheological MC model gives rise to high viscosity, usually the time step is not restricted by the viscous effect.

In three-dimensional SPH simulations of large-scale landslides, due to the problem scale and the complex terrain, the number of SPH particles can easily exceed one million. If one needs to investigate the convergence of SPH simulations, even more particles should be used. In such cases, numerical efficiency is of great concern. Simulations based on serial computing or parallel computing with a few CPU cores would need prohibitively long time to finish. Therefore, massively parallel computing is essential for three-dimensional SPH simulations of large-scale landslides. Recent developments of GPU-acceleration techniques allow massively parallel computing using easily available cost and energy effective hardware. The latest GPU-accelerated SPH solvers can efficiently simulate millions to dozens of millions particles with a single GPU device installed on a conventional desktop [28, 55, 64].

In this work, the aforementioned constitutive models and formulations are implemented in the open-source GPU-accelerated SPH solver LOQUAT, which already includes an elastoplastic Drucker-Prager (DP) model. Readers interested in implementation details can refer to [28]. The procedure of computations with rheological models follows the same process as that for elastoplastic DP model, except that in each step one additional round of particle interaction is required to compute the shear rate and then the apparent viscosity using the rheological MC model.

5. BAIGE LANDSLIDE AND NUMERICAL MODEL

In this work, all simulations and analyses are based on the real case of Baige landslide. The convergence of SPH, performance of different formulations and influences of model parameters are investigated by comparing numerical results with field data. In this section, we briefly introduce the Baige landslide and the process of generating 3D SPH computational model.

© The Author(s) or their Institution(s)

5.1. *The Baige landslide*

On October 11, 2018, a massive landslide occurred at the right bank of Jinsha River (31° 4′ 56.41″ N, 98° 42′ 17.98″ E), near Baige village located at the border of Sichuan Province and Tibet Autonomous Region in southwest of China (see Figure 1(a)) [65–67]. In this area, a series of NNW-trending faults or folds in the strata are well developed (for example the Boluo-muxie fault F_{14}) due to multi-phase tectonic movements in the freeze-thaw plateau. The lithology of the strata is quite complex, which mainly composed of plagioclase gneiss, rock fragment sandstone, granodiorite, and serpentine [68]. The average and maximum annual precipitations in the landslide area are 650 mm and 1067.7 mm, respectively [69]. However the cumulative rainfall already exceeded 590 mm between middle June and early October, 2018 according to the nearest rainfall monitoring station. Persistent heavy rainfall resulted in high water content or saturation of bed deposits, which is considered as the primary factor triggering the dramatic failure. During the landslide, large rock masses rushed into the Jinsha River and blocked the channel (Fig. 1b). The total volume of Baige landslide is approximately 27.6 million m^3 [65].

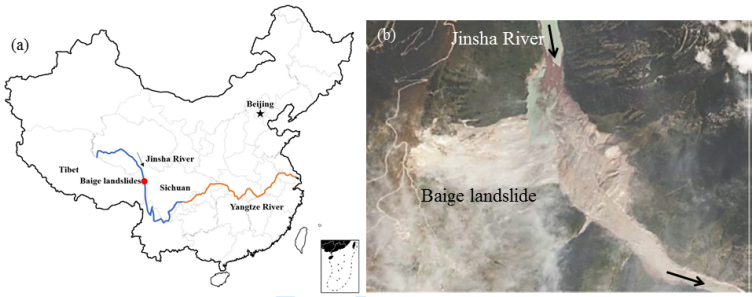

Figure 1: (a) Location and (b) oblique photograph (b: credit by Yangtze River Water Resources Commission) of the Baige landslides (Ref. [67]).

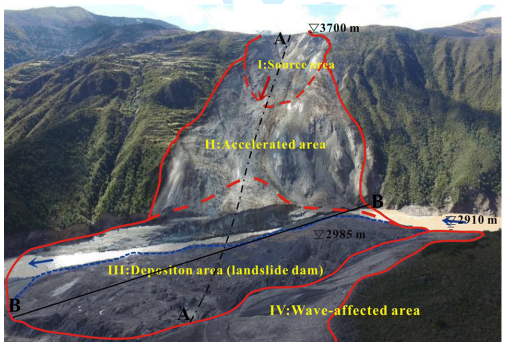

Figure 2: Overviews of the Baige landslide affected area divided into four parts: (I) the source area, (II) the acceleration area, (III) the deposition area, and (IV) the wave affected area (Ref. [70]). The height of deposit along A-A and B-B sections will be compared with numerical results in subsequent analyses.

The Baige landslide area can be generally divided into four parts (Figure 2): (I) The source area (0.48 million m^2), originally with several to tens of meters of loose fluvial sediments and glacial deposits on the surface slope of mountaintop; (II) The acceleration area (0.33 million m^2) below the source area, located in the middle of the slope. This area is mainly defined by the speed-up of landslide. The landslide mass slides along the slope surface with a high kinetic energy, eroding the pre-existing loose materials by scraping; (III) The fan-shape deposition area (0.54 million m^2) is the main accumulation space of debris materials due to the deceleration of avalanches at the toe of mountain. The longitudinal of the deposit area is parallel to the river channel. The bottom length and the top width of the deposit fan are about 1500 m and 700 m, respectively [67]. The average and maximum heights of the deposit fan are 40 m and 85 m, respectively [71]; (IV) The wave-affected area (0.32 million m^2) is situated on the left-side of the river. The massive high-speed sliding mass rushed into Jinsha River and caused a 160 m high surge wave [69]. The

© The Author(s) or their Institution(s)

landslide-generated surge strongly impacts the riverbed and the left bank, leaving a large scar of 150-200 m in height and more than 1000 m in length.

5.2. Generation of SPH model

In SPH simulations, both the moving materials and the fixed bed rock are modelled as particles representing material element with fixed mass. The 3D terrain topographies before and after the landslide are available in the form of Digital Elevation Models (DEMs). With these DEMs, the realistic topography of the boundary and the initial location of the sliding mass can be obtained.

The original DEMs of Baige landslides are represented by elevation information on a regular grid with a resolution of 10 m. With the DEMs, the boundaries particles of the 3D SPH model can be conveniently generated by converting the grid points into SPH particles and assigning the corresponding coordinates and properties (mass, volume, density, etc.). Two additional layers of boundary particles are added below the original layer as required by the boundary treatment method. The sliding body is also filled with particles by keeping the same x and y coordinates as those of boundary particles but step-wisely increasing the z-coordinates. Computational models with finer resolutions can be generated by first refining the DEMs and then following the same procedure. With this method, 3D SPH models with different resolutions can be readily generated. Figure 3 shows the procedure of SPH particle generation and the final computational model.

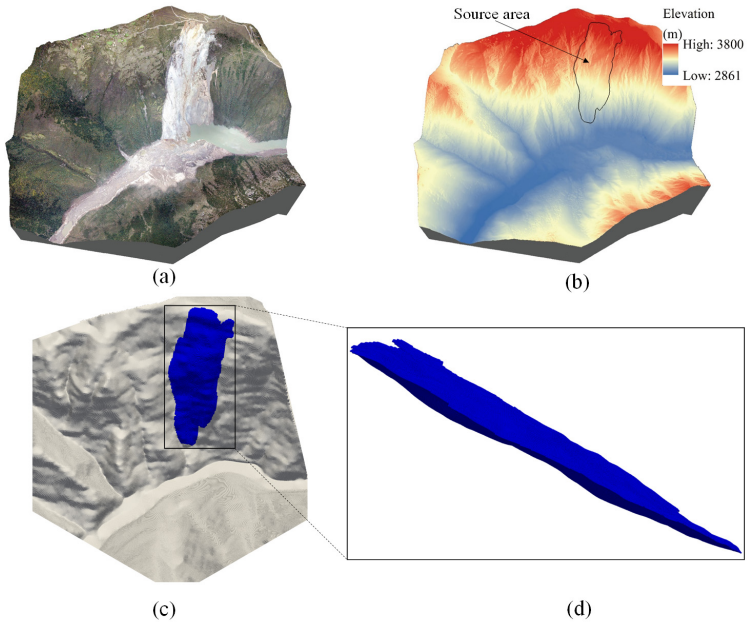

Figure 3: The procedure for SPH model generation: (a) post-failure DEM, (b) pre-failure DEM and determination of sliding body, (c) generation of SPH particles (Δr = 2 m), (d) SPH particles representing the sliding body.

6. CONVERGENCE ANALYSIS

As mentioned before, SPH has been employed in 2D and 3D modelling of large-scale landslides [29–33]. However, the role of numerical resolution has rarely been investigated. If numerical resolution has great influence on the results, one needs to employ a resolution that produces converged results. This is to ensure that the numerical results are physically correct and to eliminate the uncertainties induced by the different resolutions. For instance, if we perform a simulation with only a single resolution, and luckily, the numerical results agree well with field data. We cannot say that the results are reliable and reflect the real physics, because this agreement might be pure coincidental

© The Author(s) or their Institution(s)

and with a different resolution it might cease to exist. Consequently, in this section we will investigate the influence of numerical resolution and the convergence property of SPH modelling of large-scale landslides.

The Baige landslide is used as a benchmark for the investigation. Five numerical models, with particle sizes Δr = 10.0 m, 5.0 m, 3.3 m, 2.5 m and 2.0 m, are created based on the DEMs before and after the landslide. The resulted particle numbers of the five numerical models are listed in Table 1. In the convergence analysis, the sliding mass is modelled using the rheological MC model with parameters of μ = 0.2, c = 4.0 kPa, and m = 100 s^{-1}. The reason of selecting this set of parameters will be discussed in the next section on parameter study.

Table 1. Number of SPH particles in the five numerical models

Particle size (m)	Boundary	Material	Total
10.0	242,454	25,045	267,499
5.0	971,643	191,073	1,162,716
3.3	2,187,558	633,720	2,821,278
2.5	3,890,199	1,489,277	5,379,476
2.0	6,392,106	2,893,170	9,285,276

The whole flow process in the simulations lasts around 100 s. The final deposits obtained in the five simulations are shown in Figure 4. For comparison, the deposition area obtained from field investigation is also plotted. Generally, the flow dynamics obtained from simulations with different resolutions are similar: the failed mass slides down the right slope of the valley, runs up along the left slope, and spreads up- and downstream, resulting in similar shapes of deposition. However, the run-outs from the five simulations are different. It is found that a simulation with finer SPH particle size generally gives rise to longer run-outs in both the directions of sliding and river flow. This observation is expectable, because the particle size determines the thickness of the basal shear zone, in which the friction contact between sliding mass and the bedrock plays a major role in the energy dissipation and final depositing. If same material properties are considered, a thicker shear zone requires larger force to deform and dissipates more energy during plastic deformation, which is similar to the mesh-dependency in finite element simulation of strain localization [72]. In SPH modelling of large-scale landslides, this particle size-dependency has a strong impact on the run-out and final deposition. From Figure 4, it can be observed that the deposition area from low resolution (Δr = 10.0 m) is significantly smaller than that of high resolution (Δr = 2.0 m). Another observation is that the change of deposition area is obvious when the particle size decreases from 10.0 m to 3.3 m, but the difference between results with particle size from 3.3 m to 2.0 m is insignificant. This means that in the simulation of Baige landslide converged results can be achieved with particle size equal to or smaller than 3.3 m.

This convergence behaviour can also be demonstrated quantitatively using the error in deposition area. The error is defined as

$$e = \frac{|A_{field} - A_{num}|}{A_{field}} \tag{24}$$

where A_{field} and A_{num} are the deposition areas obtained from field investigation and numerical simulation, respectively. Figure 5 gives change of error in deposition area with respect to total particle number. It is found that when the total particle number is smaller than 2.8 million, the error decreases quickly with the increasing particle number. Once the total particle number is larger than 2.8 million, further refining the numerical model leads to drastic increase of total particle number (from 2.8 to 9.3 millions); however, the error of deposition area remains more or less the same. This means numerical convergence is achieved when the particle size is smaller than 3.3 m. Notably, unconverged and converged results has significant difference. For instance, the area obtained from the simulation with Δr = 10.0 m has an error of 36%, whereas the converged results only has an error of 15%. This relatively large difference proves the necessity to perform convergence analysis to select the appropriate numerical resolution before further investigations such as parameter study, comparison of numerical formulations and constitutive model, and back analysis.

Numerical resolution also has strong influence on the height of deposit. Figure 6 shows the deposition height along the A-A and B-B sections obtained from the five simulations (The locations of A-A and B-B sections are shown in Figure 2). The field data obtained by comparing the pre- and post-failure terrain is also plotted. It is found that the general trend is that simulations with smaller particle sizes produces depositions with lower depth and wider spread. The convergence behaviour can also be clearly observed in the results of deposition height. The results from

© The Author(s) or their Institution(s)

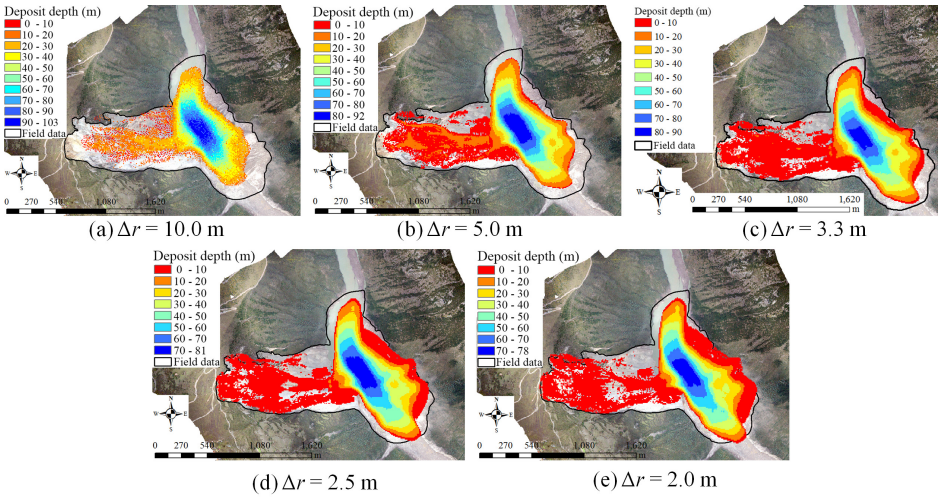

Figure 4: The final depositions from simulations with different numerical resolutions. The black line indicates the area of deposition obtained from field investigation.

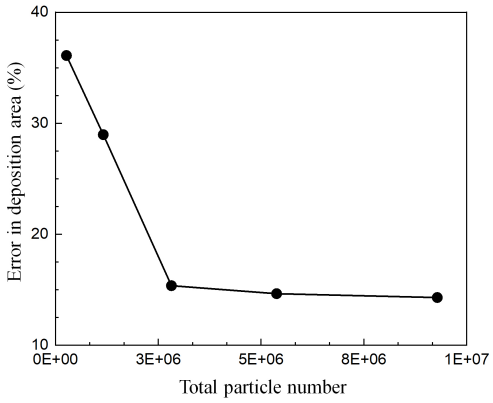

Figure 5: The relation between total particle number and error in deposition area.

simulations with 10.0 m and 5.0 m particle sizes are rather different from those with particle sizes from 3.3 m to 2.0 m. The profile of deposition height changes greatly when particle size varies from 10.0 m to 3.3 m, but does not show significant difference in simulations with particle size equal to or smaller than 3.3 m. This observation is in consistent with previous analysis on the deposition area, confirming that in the SPH modelling of Baige landslide, the particle size Δr = 3.3 m is sufficiently fine to achieve numerical convergence.

From Figure 6 it is also found the converged numerical results generally represent the real deposition behaviour in terms of the maximum deposition height and run-out. However, there are still non-negligible discrepancies between the converged numerical results and the field data. The possible reasons of the discrepancies may be twofold: (1) The incomplete consideration of material behaviour. Natural geomaterials are complex non-homogenous multiphase material. The applied rheological MC model can only account for the friction behaviour in a single-phase homogeneous fashion. However, other aspects such as the presence of large boulders and dynamic viscous effect may also have impact on the mass movement. These aspects are not considered in the present modelling. (2) The river water is not considered in the simulation but it may have impact on the landslide by preventing the material running up the left bank and allowing longer run-out in the downstream direction.

From the convergence analysis it is found that in SPH modelling of large-scale landslides it is important to select a sufficiently small particle size to get reliable results free from uncertainties induced by numerical resolution. Although

© The Author(s) or their Institution(s)

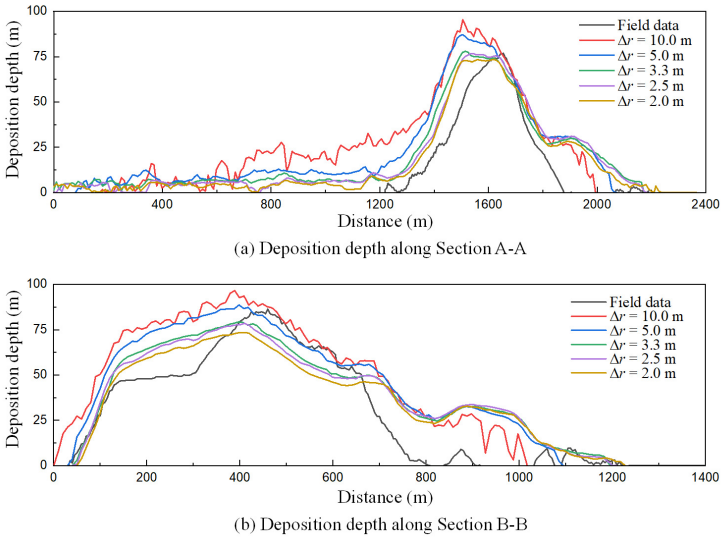

Figure 6: The deposition depths along sections A-A and B-B obtained from simulations with different numerical resolutions.

the convergence analysis shows that in Baige landslide $\Delta r = 3.3$ m is sufficient, this value might not be universally applicable for large-scale landslides. Because the convergent numerical resolution depends on many factors such as problem size and geometry. Therefore, when performing SPH modelling of large-scale landslides, a separate convergence analysis is recommended to select the proper numerical resolution. A difficulty caused by a sufficiently small particle size is the large number of SPH particles in numerical model, which severely reduce numerical efficiency. This difficulty needs to be tackled using massive parallelization, such as GPU acceleration employed in this work.

7. PARAMETER STUDY

In numerical simulations, the mechanical properties are accounted for using constitutive models; therefore, the model parameters determine the material responses and have decisive impact on numerical results. In this section, the influence of parameters of the widely-used rheological MC model are investigated. Three parameters are investigated, i.e., c, μ, and m. As discussed before, the influence of plastic viscosity η_∞ can be neglected because the viscosity resulted from friction and cohesion is often several orders larger. All simulations in the parameter study employ the numerical resolution of $\Delta r = 3.3$ m, which results in converged modelling according to previous analysis.

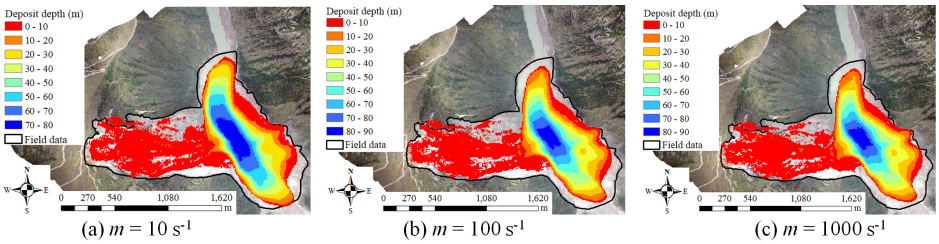

Figure 7: The depositions from simulations with different parameter m.

7.1. Influence of regularization parameter m

Different from the physical parameters c and ϕ, the regularization parameter m is purely numerical. It is employed to prevent singularity induced by extremely slow deformation where $\dot{\gamma}$ is close to zero. A larger m results in material

© The Author(s) or their Institution(s)

response closer to the original rheological MC model; therefore, theoretically a sufficiently large m should be selected. However, a large m leads to extremely large apparent viscosity in quasi-static flow regions hence severely reduces the numerical efficiency, as demonstrated in Eq. (23). Therefore, in numerical simulations it is usually required to select a value of m as small as possible while at the same time guarantee physically correct results [63]. Becker and Idelsohn employed $m = 10^4$ s^{-1} in implicit finite element modelling [7]. However, this value is prohibitively high in explicit SPH modelling. For instance, if we assume a sliding body which has a depth of 50 m, a density of 2000 kg/m^3, a frictional coefficient of 0.2 and cohesion of 0 kPa. According to the constitutive model Eq. (11), in the quasi-static flow regime, the estimated viscosity is around 2.0×10^9 Pa·s at the bottom. For a simulation with numerical resolution $\Delta r = 3.3$ m, the resulted time step is in the order of 10^{-6} s. For modelling of large-scale landslides, this time step is rather small, leading to very long simulation time despite that the massive GPU parallelization is employed. In this section, the proper value of m for SPH modelling of large-scale landslides will be investigated through parameter study.

Three simulations with varying m of 10, 100, 1000 s^{-1} are carried out. Other parameters are the same for the three simulations: $\Delta r = 3.3$ m, $c = 4.0$ kPa, $\mu = 0.2$. The obtained final depositions are shown in Figure 7. It can be observed that the shapes of deposition from simulations with $m = 100$ and 1000 s^{-1} are almost the same, while the deposition area from $m = 10$ s^{-1} is slightly larger. This trend can be confirmed by the deposition height along the A-A and B-B sections, as shown in Figure 8. The deposition from $m = 10$ s^{-1} has lower maximum depth and flatter shape, indicating that the mobility of the mass is higher. This is because that $m = 10$ s^{-1} is too small and cannot produce large enough viscosity to account for the original material behaviour in the quasi-static regime. On the other hand, the results from $m = 100$ and 1000 s^{-1} are almost the same, which means that $m = 100$ s^{-1} is sufficiently large in SPH modelling of large-scale landslides. Further increasing m does not give rise to more physical results but increases the risk of excessively large viscosity which may restrict the numerical efficiency.

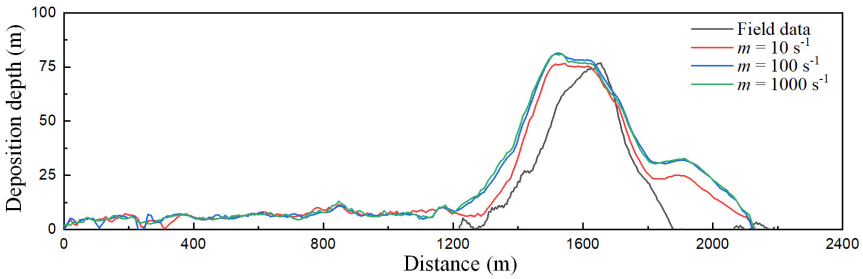

(a) Deposition depth along Section A-A

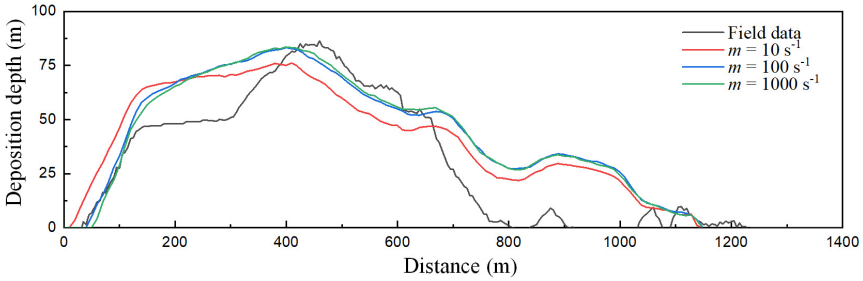

(b) Deposition depth along Section B-B

Figure 8: The deposition depth along sections A-A and B-B from simulations with different parameter m.

Note that the value $m = 100$ s^{-1} is appropriate for SPH modelling of large-scale landslides usually with flow depth more than 10 m. For small-scale laboratory problems, e.g. the collapse of sand pile [7], this relatively small value might not be sufficient [63].

© The Author(s) or their Institution(s)

7.2. *Influence of cohesion c*

The yield stress in the rheological MC model is computed based on the Mohr-Coulomb criterion, which employs the cohesion c and friction coefficient μ to account for the yield behaviour of the sliding mass. For natural geomaterials in landslides, typical value of cohesion ranges from 0 to 30 kPa [30, 31, 73]. To investigate the influence of cohesion c on the landslide run-out and deposition, we performed four simulations with c = 0, 10, 20, 30 kPa, with other parameters fixed as: Δr = 3.3 m, m = 100 s^{-1}, and μ = 0.2.

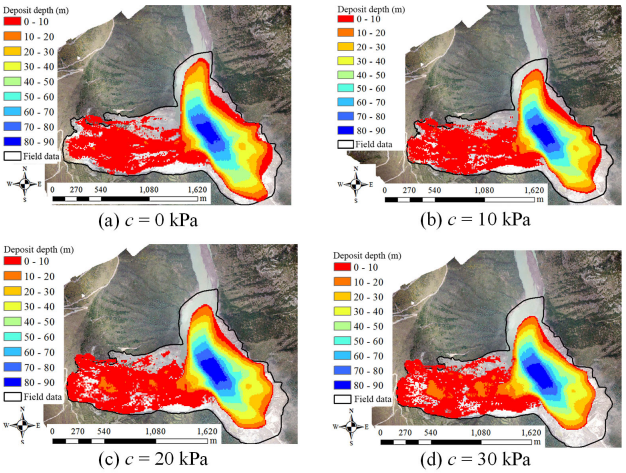

Figure 9: The depositions from simulations with different cohesion c.

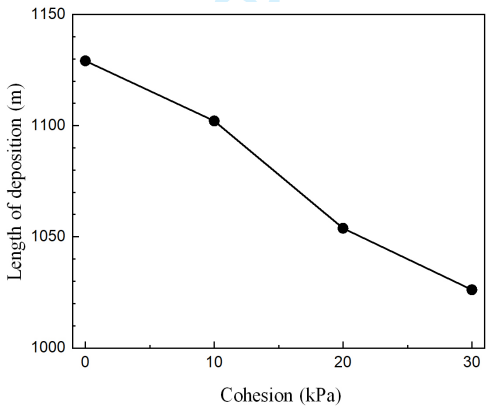

Figure 10: The relation between cohesion c and the length of final deposition along B-B.

The final deposition pattern from the four simulations are given in Figure 9. Obviously, a larger cohesion results in smaller run-out and deposition area. In the range of common value of cohesion, from 0 to 30 kPa, the length of the deposition along the section B-B decreases from 1129.2 to 1026.2 m. As shown in Figure 10, the length changes almost linearly with respect to cohesion. The difference between the maximum and minimal lengths is 9.12%, which is relatively small considering that the cohesion changes through the full range of common value.

The height of deposits along the A-A and B-B sections obtained with varying cohesion is shown in Figure 11. It is found that when the cohesion increases from 0 to 30 kPa, the results are almost the same in terms of maximum height and general deposition pattern. Notable differences can be found only near the edge of deposits. The reason is that in large-scale landslides, the height of sliding mass is usually very large, resulting in high normal stresses. Consequently, the major contribution of the yield stress is friction, whereas the effect of cohesion is negligible compared with friction.

© The Author(s) or their Institution(s)

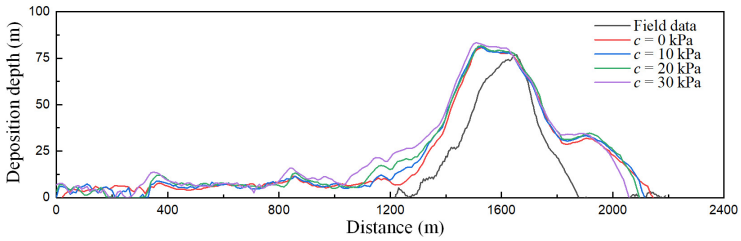

(a) Deposition depth along Section A-A

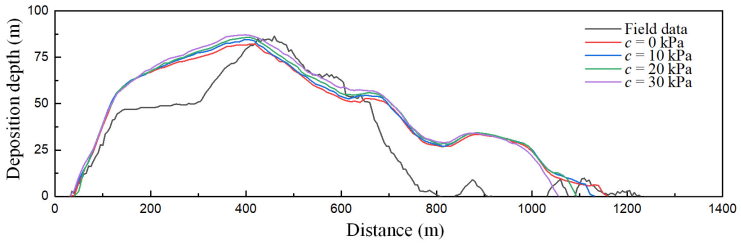

(b) Deposition depth along Section B-B

Figure 11: The height of deposit along sections A-A and B-B from simulations with different cohesion c.

The cohesion only plays a significant role near the edge of deposits. Because near edges the material height is small and the friction effect is not large enough to eclipse the effect of cohesion. This is like the difference between small-scale and large-scale problems. In small-scale problems, the cohesion is very important and largely decides the final deposition [10]; however, in large-scale landslides, cohesion plays a less significant role.

From the parameter study, it is found generally higher cohesions result in lower run-outs and smaller deposition areas. However, the influence of cohesion is relatively limited. When it varies within the natural range, the difference in run-out is less than 10%. Besides, it almost has no influence in areas with large deposition height and only affects the depositing behaviour near fronts and rears of landslides.

7.3. Influence of friction coefficient μ and scale effect in large-scale landslides

Natural geomaterials in landslides usually have frictional angle between 20° and 40° [73], corresponding to frictional coefficient between 0.36 to 0.84. Indeed, in previous SPH modelling of large-scale landslides, the friction angle is usually taken as 30° [30, 31], equivalent to a frictional coefficient of 0.58. It is found in small-scale problems, when applying the common friction coefficient in SPH computing, satisfactory results well-corroborated by experiments can be obtained [10, 11, 26, 28, 55, 74]. However, it is generally observed that large-scale landslides have run-outs much longer than expected from the usual values of friction coefficient [41–43], indicating that the effective friction in large sliding mass is smaller than those obtained in laboratory tests. The mechanism of this friction weakening in large-scale landslides has already been a subject of long discussion, yet a determinative explanation has not been reached [43]. Nevertheless, the presence of friction weakening effect means that if the usual values of friction coefficient are employed in numerical simulation of large-scale landslides, the predicted run-outs and deposition areas would be severely underestimated. The influence of friction coefficient and the scale-related friction weakening effect will be investigated in this section.

Four simulations with friction coefficients $\mu = 0.1$, 0.2, 0.3, and 0.4 are carried out, with other parameters taken as $\Delta r = 3.3$ m, $m = 100$ s^{-1}, $c = 4$ kPa. The final deposits from the four simulations are shown in Figure 12. It is found that the friction coefficient has significant influence on the run-out and deposition area. With different friction coefficient, the dynamics of the mass movement differs significantly. When the friction coefficient is taken as 0.1, the failed mass slides down the right slope, climbs up the left slope, and spreads far away in the up- and downstream directions. The deposit has low height but large area. In the simulation with $\mu = 0.4$, on the other hand, the mass accumulates at the foot of the right slope, resulting in deposit with large height but small spread area. Obviously, the friction coefficient has the greatest influence on large-scale landslides among all model parameters. This observation is

© The Author(s) or their Institution(s)

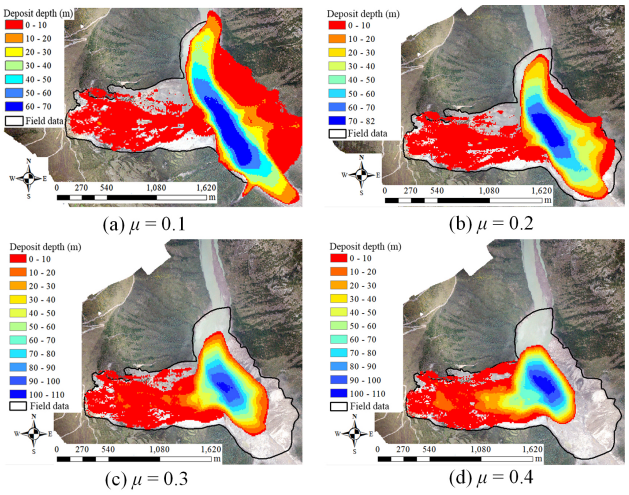

Figure 12: The deposits from simulations with different friction coefficient μ

unsurprising, because in large-scale landslides, the yield stress is mainly dependent on friction due to the high normal stress. The change of deposition length along the B-B section is shown in Figure 13. The length almost linearly decreases from 1300.8 m to 715.6 m as the friction coefficient increases from 0.1 to 0.4. This extent of change is much larger than that obtained by changing the cohesion. Note that $\mu = 0.4$ is a rather low friction coefficient for natural geomaterials [73]; however, even with this low friction coefficient, the simulated run-out and deposition area are much smaller than those observed in field. This indicates that in the real event the effective friction is much less than that obtained from field and laboratory tests based on the deposition materials.

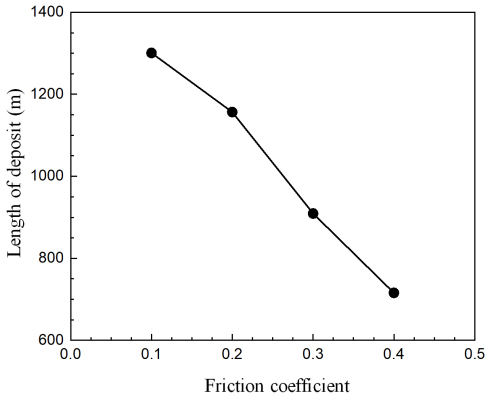

Figure 13: The relation between friction coefficient μ and the length of final deposit along B-B

The height of final deposit along the A-A and B-B sections is given in Figure 14. Consistent with the observations from Figure 12, a higher friction coefficient gives rise to larger maximum heigh and smaller deposition area. The deposition height changes significantly in simulations with different friction coefficient, indicating that the friction coefficient has the greatest influence on the mass flow process among all model parameters.

From the parameter study on friction coefficient, it is found that the results obtained with $\mu = 0.2$ have the best agreement with field data. $\mu = 0.2$ corresponds to a friction angle of 11.3°, which is much lower than the friction angle of geomaterials obtained from field investigations and laboratory tests. The SPH simulations confirm the existence of friction weakening effect in large-scale landslides. Consequently, in SPH modelling of large-scale landslides, the friction coefficient should be carefully determined to obtain reliable results. Reduction of the laboratory-based friction coefficient is required, by either selecting values from empirical parameter range, or employing velocity-based

© The Author(s) or their Institution(s)

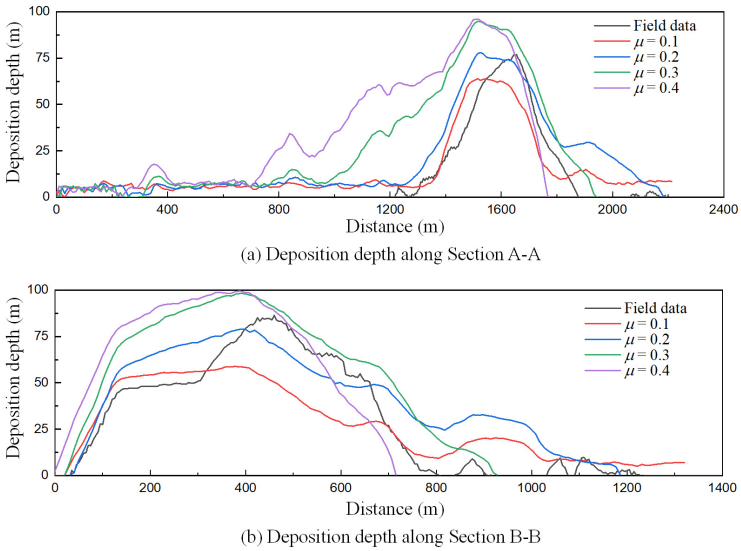

Figure 14: The height of deposit along sections A-A and B-B from simulations with varying friction coefficient μ.

reduction relations [43, 45].

8. COMPARISON BETWEEN DIFFERENT FORMULATIONS

As discussed in Section 3.3, the momentum equation can be solved using full stress tensor or by direct discretization of the viscous Laplacian term. The difference between these two approaches, as well as the difference between different Laplacian discretizations, have not been investigated in literature. In this section, the performance of four formulations described in Section 3, i.e. LF-Morris, LF-Hérault, LF-Shao, and SF are compared. Four simulations are carried out with the following parameters: particle size Δr = 3.3 m, m = 100 s^{-1}, c = 4 kPa, μ = 0.2. Except for the formulation for discretizing the momentum equation, all computation conditions are the same in the four simulations.

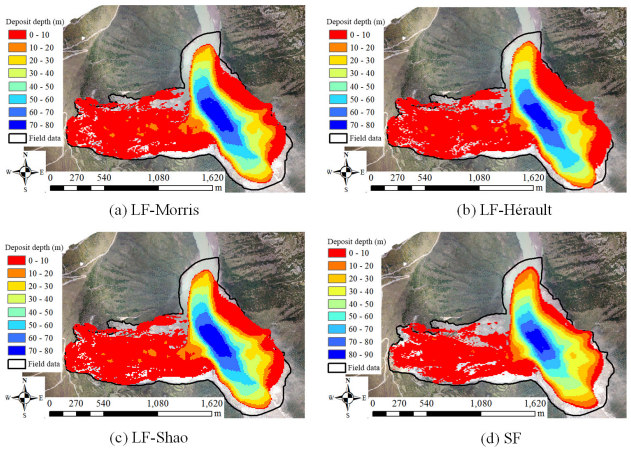

Figure 15: The deposits from simulations with different SPH formulations.

Figure 15 shows the final deposits from the four simulations. It is found that all four formulations give similar results. Generally, Simulations using direct Laplacian discretizations show slightly larger deposition area (Figure 15(a) - (c)), whereas stress-based formulation results in smaller deposit (Figure 15(d)). Among the Laplacian formulations,

© The Author(s) or their Institution(s)

the LS-Morris and LS-Shao gives almost identical results, while LS-Hérault results in the largest deposit among the four simulations. Table 2 gives the area of deposit obtained from the four simulations. It is found that the difference between the largest (LF-Hérault) and the smallest (SF) is around 15%. Among the Laplacian-based formulations, the deposit area from LF-Hérault is 8% bigger than that from LF-Morris. These observations indicate that using different formulations has obvious impact on simulation results, which is overlooked in previous studies.

Table 2. Summary of the simulations with the four formulations

Formulation	Deposit area (km^2)	GPU memory consumption (MB)	FPS
LF-Morris	0.733	817	22.88
LF-Hérault	0.804	817	22.44
LF-Shao	0.738	817	21.54
SF	0.697	979	18.07

The performance of the four simulations in terms of computational cost is also investigated. Table 2 summarizes the GPU memory consumption and numerical efficiency. The efficiency is measured using frame per second (FPS), which is the average number of computational steps executed in one second of wall-clock time [75]. It can be observed that all three Laplacian-based formulations need the same amount of memory, which is around 20% less compared to that consumed by the stress-based formulation. In terms of efficiency, the three Laplacian-based formulations are faster than the stress-based formulation. The fastest one (LF-Morris) is about 26% faster than the stress-based formulation. This is not surprising, because the Laplacian-based formulations does not use full stress tensors; thus, they avoid all operations and computations associated with stress tensors. Among the three Laplacian-based formulations, the original Morris type has simplest form; thus, it has the highest efficiency.

In SPH modelling of landslides and geophysical flows, the stress-based formulation is probably the most widely used [29–33]. Based on the aforementioned analysis, however, it seems that the LF-Morris formulation is an optimal choice for SPH modelling of large-scale landslides, as it has lower memory consumption and higher efficiency. Furthermore, it gives results very close to those of the stress-based formulation.

Draft

9. CONCLUSIONS

In this paper, several issues on SPH modelling of large-scale landslides are investigated using a GPU-accelerated SPH solver. The Baige landslide is employed as a benchmark. Based on our analysis, the following conclusions can be drawn.

(1) Numerical resolution has significant influence on SPH simulation results. When performing SPH modelling of large-scale landslides, an additional convergence study should be performed to select a proper numerical resolution. In the Baige landslide, a particle size $\Delta r = 3.3$ m is fine enough; however, this value may not be universally applicable.

(2) Among the three parameters of the rheological MC model, the friction coefficient μ has the greatest influence, which largely determines the flow dynamics and final deposition. The cohesion c only has significant influence in areas with small material depth, e.g. fronts or rears of landslides, but is negligible in areas with large material depth. As for the numerical coefficient m, values in the magnitude of 10^2 are sufficient for SPH modelling of large-scale landslides.

(3) It is confirmed in our investigation that large-scale landslides have considerable scale effect. Friction coefficients obtained from laboratory tests can accurately predict small-scale mass flows; however, when they are employed in modelling of large-scale landslides, significant underestimation of run-outs can be observed. This indicates that in large-scale landslides there exist unrevealed mechanisms leading to significant friction reduction, which should be considered in SPH modelling.

(4) Both stress- and Laplacian-based formulations give rise to satisfactory simulation. However, it is found that the original Morris-type Laplacian formulation has lower memory consumption and higher numerical efficiency.

© The Author(s) or their Institution(s)

ACKNOWLEDGMENT

The authors would like to thank the funding from the Natural Science Foundation of China (51709230 and 42007270), EU Horizon 2020 RISE projects HERCULES (778360) and FRAMED (734485), and the Nazarbayev University Research Fund (SOE2017001).

References

[1] N Prime, F Dufour, and F Darve. Solid–fluid transition modelling in geomaterials and application to a mudflow interacting with an obstacle. *International Journal for Numerical and Analytical Methods in Geomechanics*, 38(13):1341–1361, 2014.

[2] M Pastor, B Haddad, G Sorbino, S Cuomo, and V Drempetic. A depth-integrated, coupled SPH model for flow-like landslides and related phenomena. *International Journal for Numerical and Analytical Methods in Geomechanics*, 33(2):143–172, 2009.

[3] C M Mast. *Modeling landslide-induced flow interactions with structures using the material point method*. PhD thesis, University of Washington, 2013.

[4] G Marcato, M Mantovani, A Pasuto, L Zabuski, and L Borgatti. Monitoring, numerical modelling and hazard mitigation of the Moscardo landslide (Eastern Italian Alps). *Engineering Geology*, 128:95–107, 2012.

[5] A Leonardi, F K Wittel, M Mendoza, R Vetter, and H J Herrmann. Particle–fluid–structure interaction for debris flow impact on flexible barriers. *Computer-Aided Civil and Infrastructure Engineering*, 31(5):323–333, 2016.

[6] F Salazar, J Irazábal, A Larese, and E Oñate. Numerical modelling of landslide-generated waves with the particle finite element method (PFEM) and a non-Newtonian flow model. *International Journal for Numerical and Analytical Methods in Geomechanics*, 40(6):809–826, 2016.

[7] P A Becker and S R Idelsohn. A multiresolution strategy for solving landslides using the Particle Finite Element Method. *Acta Geotechnica*, 11(3):643–657, 2016.

[8] J J Monaghan. Simulating free surface flows with SPH. *Journal of Computational Physics*, 110(2):399–406, 1994.

[9] D Violeau and B D Rogers. Smoothed particle hydrodynamics (SPH) for free-surface flows: past, present and future. *Journal of Hydraulic Research*, 54(1):1–26, 2016.

[10] H H Bui, R Fukagawa, K Sako, and S Ohno. Lagrangian meshfree particles method (SPH) for large deformation and failure flows of geomaterial using elastic–plastic soil constitutive model. *International Journal for Numerical and Analytical Methods in Geomechanics*, 32(12):1537–1570, 2008.

[11] C Peng, W Wu, H S Yu, and C Wang. A SPH approach for large deformation analysis with hypoplastic constitutive model. *Acta Geotechnica*, 10(6):703–717, 2015.

[12] M B Liu, G R Liu, and K Y Lam. Adaptive smoothed particle hydrodynamics for high strain hydrodynamics with material strength. *Shock Waves*, 15(1):21–29, 2006.

[13] J Limido, C Espinosa, M Salaün, and J Lacome. SPH method applied to high speed cutting modelling. *International Journal of Mechanical Sciences*, 49(7):898–908, 2007.

[14] S Chakraborty and A Shaw. A pseudo-spring based fracture model for SPH simulation of impact dynamics. *International Journal of Impact Engineering*, 58:84–95, 2013.

[15] M R I Islam and C Peng. A Total Lagrangian SPH method for modelling damage and failure in solids. *International Journal of Mechanical Sciences*, 157:498–511, 2019.

[16] M B Liu, G R Liu, K Y Lam, and Z Zong. Smoothed particle hydrodynamics for numerical simulation of underwater explosion. *Computational Mechanics*, 30(2):106–118, 2003.

[17] M B Liu, G R Liu, Z Zong, and K Y Lam. Computer simulation of high explosive explosion using smoothed particle hydrodynamics methodology. *Computers & Fluids*, 32(3):305–322, 2003.

[18] G R Johnson, R A Stryk, and S R Beissel. SPH for high velocity impact computations. *Computer Methods in Applied Mechanics and Engineering*, 139(1-4):347–373, 1996.

[19] J Y Chen, C Peng, F S Lien, E Yee, and X H Zhao. Simulations for the explosion in a water-filled tube including cavitation using the SPH method. *Computational Particle Mechanics*, 6(4):515–527, 2019.

[20] L Cascini, S Cuomo, M Pastor, G Sorbino, and L Piciullo. SPH run-out modelling of channelised landslides of the flow type. *Geomorphology*, 214:502–513, 2014.

[21] M Pastor, T Blanc, B Haddad, S Petrone, M S Morles, V Drempetic, D Issler, G B Crosta, L Cascini, and G Sorbino. Application of a SPH depth-integrated model to landslide run-out analysis. *Landslides*, 11(5):793–812, 2014.

[22] M Pastor, A Yague, M M Stickle, D Manzanal, and P Mira. A two-phase SPH model for debris flow propagation. *International Journal for Numerical and Analytical Methods in Geomechanics*, 42(3):418–448, 2018.

[23] A M Abdelrazek, I Kimura, and Y Shimizu. Simulation of three-dimensional rapid free-surface granular flow past different types of obstructions using the SPH method. *Journal of Glaciology*, 62(232):335–347, 2016.

[24] C Peng, X G Guo, W Wu, and Y Q Wang. Unified modelling of granular media with smoothed particle hydrodynamics. *Acta Geotechnica*, 11(6):1231–1247, 2016.

[25] L Minatti and E Paris. A SPH model for the simulation of free surface granular flows in a dense regime. *Applied Mathematical Modelling*, 39(1):363–382, 2015.

[26] W Chen and T Qiu. Numerical simulations for large deformation of granular materials using smoothed particle hydrodynamics method. *International Journal of Geomechanics*, 12(2):127–135, 2012.

[27] E Kermani and T Qiu. Simulation of quasi-static and dynamic collapses of rectangular granular columns using smoothed particle hydrodynamics method. *International Journal of Geomechanics*, 18(9):04018113, 2018.

© The Author(s) or their Institution(s)

[28] C Peng, S Wang, W Wu, H S Yu, C Wang, and J Y Chen. LOQUAT: an open-source GPU-accelerated SPH solver for geotechnical modeling. *Acta Geotechnica*, 14(5):1269–1287, 2019.
[29] Y Huang, W J Zhang, Q Xu, P Xie, and L Hao. Run-out analysis of flow-like landslides triggered by the Ms 8.0 2008 Wenchuan earthquake using smoothed particle hydrodynamics. *Landslides*, 9(2):275–283, 2012.
[30] M Hu, M B Liu, M W Xie, and G R Liu. Three-dimensional run-out analysis and prediction of flow-like landslides using smoothed particle hydrodynamics. *Environmental Earth Sciences*, 73(4):1629–1640, 2015.
[31] Z L Dai, Y Huang, H L Cheng, and Q Xu. 3D numerical modeling using smoothed particle hydrodynamics of flow-like landslide propagation triggered by the 2008 Wenchuan earthquake. *Engineering Geology*, 180:21–33, 2014.
[32] Z L Dai, Y Huang, H L Cheng, and Q Xu. SPH model for fluid–structure interaction and its application to debris flow impact estimation. *Landslides*, 14(3):917–928, 2017.
[33] C Q Zhu, Y Huang, and L T Zhan. SPH-based simulation of flow process of a landslide at Hongao landfill in China. *Natural Hazards*, 93(3):1113–1126, 2018.
[34] W Wang, G Q Chen, Z Han, S H Zhou, H Zhang, and P D Jing. 3D numerical simulation of debris-flow motion using SPH method incorporating non-Newtonian fluid behavior. *Natural Hazards*, 81(3):1981–1998, 2016.
[35] H A Barnes, J F Hutton, and K Walters. *An introduction to rheology*, volume 3. Elsevier, Oxford, 1989.
[36] J P Morris, P J Fox, and Y Zhu. Modeling low Reynolds number incompressible flows using SPH. *Journal of Computational Physics*, 136(1):214–226, 1997.
[37] A Hérault, G Bilotta, A Vicari, E Rustico, and C Del Negro. Numerical simulation of lava flow using a GPU SPH model. *Annals of Geophysics*, 54(5), 2011.
[38] K Szewc. Smoothed particle hydrodynamics modeling of granular column collapse. *Granular Matter*, 19(1):3, 2017.
[39] W Brian D and H E Huppert. Long–runout rockfalls. *Geology*, 26(9):803–806, 1998.
[40] O Pouliquen. Scaling laws in granular flows down rough inclined planes. *Physics of fluids*, 11(3):542–548, 1999.
[41] A Lucas and A Mangeney. Mobility and topographic effects for large Valles Marineris landslides on Mars. *Geophysical Research Letters*, 34(10), 2007.
[42] L Staron and E Lajeunesse. Understanding how volume affects the mobility of dry debris flows. *Geophysical Research Letters*, 36(12), 2009.
[43] A Lucas, A Mangeney, and J P Ampuero. Frictional velocity-weakening in landslides on Earth and on other planetary bodies. *Nature Communications*, 5(1):1–9, 2014.
[44] O Hungr and S G Evans. Entrainment of debris in rock avalanches: an analysis of a long run-out mechanism. *Geological Society of America Bulletin*, 116(9-10):1240–1252, 2004.
[45] W T Zhang, C Q Shi, Y An, S H Yang, and Q Q Liu. Viscous elastoplastic SPH model for long-distance high-speed landslide. *International Journal of Computational Methods*, 16(02):1846011, 2019.
[46] E B Pitman and L Le. A two-fluid model for avalanche and debris flows. *Philosophical Transactions of the Royal Society A: Mathematical, Physical and Engineering Sciences*, 363(1832):1573–1601, 2005.
[47] S P Pudasaini. A general two-phase debris flow model. *Journal of Geophysical Research: Earth Surface*, 117(F3), 2012.
[48] K X Whipple. Open-channel flow of Bingham fluids: applications in debris-flow research. *The Journal of Geology*, 105(2):243–262, 1997.
[49] L Calvo, B Haddad, M Pastor, and D Palacios. Runout and deposit morphology of Bingham fluid as a function of initial volume: implication for debris flow modelling. *Natural Hazards*, 75(1):489–513, 2015.
[50] S Li, C Peng, W Wu, S Wang, X Q Chen, J G Chen, G D Zhou, and B K Chitneedi. Role of baffle shape on debris flow impact in step-pool channel: an SPH study. *Landslides*, 2020.
[51] H Zhu, Y D Kim, and D De Kee. Non-Newtonian fluids with a yield stress. *Journal of Non-Newtonian Fluid Mechanics*, 129(3):177–181, 2005.
[52] H Wendland. Piecewise polynomial, positive definite and compactly supported radial functions of minimal degree. *Advances in Computational Mathematics*, 4(1):389–396, 1995.
[53] J J Monaghan. SPH without a tensile instability. *Journal of Computational Physics*, 159(2):290–311, 2000.
[54] H H Bui, R Fukagawa, K Sako, and J C Wells. Slope stability analysis and discontinuous slope failure simulation by elasto-plastic smoothed particle hydrodynamics (SPH). *Géotechnique*, 61(7):565–574, 2011.
[55] L Zhan, C Peng, B Y Zhang, and W Wu. Three-dimensional modeling of granular flow impact on rigid and deformable structures. *Computers and Geotechnics*, 112:257–271, 2019.
[56] L Brookshaw. A method of calculating radiative heat diffusion in particle simulations. In *Proceedings of the Astronomical Society of Australia*, volume 6, pages 207–210, 1985.
[57] P W Cleary. Modelling confined multi-material heat and mass flows using SPH. *Applied Mathematical Modelling*, 22(12):981–993, 1998.
[58] M Basa, N J Quinlan, and M Lastiwka. Robustness and accuracy of SPH formulations for viscous flow. *International Journal for Numerical Methods in Fluids*, 60(10):1127–1148, 2009.
[59] S D Shao and E Y M Lo. Incompressible SPH method for simulating Newtonian and non-Newtonian flows with a free surface. *Advances in Water Resources*, 26(7):787–800, 2003.
[60] C T Nguyen, C T Nguyen, H H Bui, G D Nguyen, and R Fukagawa. A new SPH-based approach to simulation of granular flows using viscous damping and stress regularisation. *Landslides*, 14(1):69–81, 2017.
[61] S Marrone, M A G D Antuono, A Colagrossi, G Colicchio, D Le Touzé, and G Graziani. δ-SPH model for simulating violent impact flows. *Computer Methods in Applied Mechanics and Engineering*, 200(13-16):1526–1542, 2011.
[62] S Adami, X Y Hu, and N A Adams. A generalized wall boundary condition for smoothed particle hydrodynamics. *Journal of Computational Physics*, 231(21):7057–7075, 2012.
[63] G Chambon, R Bouvarel, D Laigle, and M Naaim. Numerical simulations of granular free-surface flows using smoothed particle hydrodynamics. *Journal of Non-Newtonian Fluid Mechanics*, 166(12-13):698–712, 2011.
[64] A J C Crespo, J M Domínguez, B D Rogers, M Gómez-Gesteira, S Longshaw, R J F B Canelas, R Vacondio, A Barreiro, and O García-Feal. DualSPHysics: Open-source parallel CFD solver based on Smoothed Particle Hydrodynamics (SPH). *Computer Physics Communications*,

© The Author(s) or their Institution(s)

187:204–216, 2015.
[65] C J Ouyang, H C An, S Zhou, Z W Wang, P C Su, D P Wang, D X Cheng, and J X She. Insights from the failure and dynamic characteristics of two sequential landslides at Baige village along the Jinsha River, China. *Landslides*, 16(7):1397–1414, 2019.
[66] L M Zhang, T Xiao, J He, and C Chen. Erosion-based analysis of breaching of Baige landslide dams on the Jinsha River, China, in 2018. *Landslides*, 16(10):1965–1979, 2019.
[67] Q M Zhong, S S Chen, L Wang, and Y B Shan. Back analysis of breaching process of Baige landslide dam. *Landslides*, pages 1–12, 2020.
[68] H B Li, S C Qi, H Chen, H M Liao, Y F Cui, and J W Zhou. Mass movement and formation process analysis of the two sequential landslide dam events in Jinsha River, Southwest China. *Landslides*, 16(11):2247–2258, 2019.
[69] W P Wang, Y P Yin, S N Zhu, L C Wang, N Zhang, and R X Zhao. Investigation and numerical modeling of the overloading-induced catastrophic rockslide avalanche in Baige, Tibet, China. *Bulletin of Engineering Geology and the Environment*, pages 1–15, 2019.
[70] Y X Hu, Z Y Yu, and J W Zhou. Numerical simulation of landslide-generated waves during the 11 October 2018 Baige landslide at the Jinsha River. *Landslides*, pages 1–12, 2020.
[71] X M Fan, Q Xu, A Alonso-Rodriguez, S S Subramanian, W L Li, G Zheng, X J Dong, and R Q Huang. Successive landsliding and damming of the Jinsha River in eastern Tibet, China: prime investigation, early warning, and emergency response. *Landslides*, 16(5):1003–1020, 2019.
[72] L Anand, O Aslan, and S A Chester. A large-deformation gradient theory for elastic–plastic materials: strain softening and regularization of shear bands. *International Journal of Plasticity*, 30:116–143, 2012.
[73] V Tofani, G Bicocchi, G Rossi, S Segoni, M D'Ambrosio, N Casagli, and F Catani. Soil characterization for shallow landslides modeling: a case study in the Northern Apennines (Central Italy). *Landslides*, 14(2):755–770, 2017.
[74] L Zhan, C Peng, B Y Zhang, and W Wu. A sph framework for dynamic interaction between soil and rigid body system with hybrid contact method. *International Journal for Numerical and Analytical Methods in Geomechanics*, 2020.
[75] C Peng, C Bauinger, K Szewc, W Wu, and H Cao. An improved predictive-corrective incompressible smoothed particle hydrodynamics method for fluid flow modelling. *Journal of Hydrodynamics*, 31(4):654–668, 2019.

Draft

© The Author(s) or their Institution(s)